Journal of Alloys and Compounds 1007 (2024) 176496

Contents lists available at ScienceDirect

Journal of Alloys and Compounds

journal homepage: www.elsevier.com/locate/jalcom

High-pressure synthesis, structure and physical properties of two quasi-one-dimensional compounds $Ba_9Nb_{2.54}Te_{15}$ and $Ba_9Ta_{1.89}Te_{15}$

Lei Duan [a], Xiaoming Chen [a,b], Zelong Wang [b,c], Yanteng Wei [a], Jun Zhang [b,c,*], Yagang Feng [a], Shun Wang [a], Suxuan Du [a], Zhiwei Zhao [a], Changjiang Xiao [a], Xiancheng Wang [b,c,*], Changqing Jin [b,c,d,*]

[a] School of Materials Science and Engineering, Henan University of Technology, Zhengzhou 450007, China
[b] Beijing National Laboratory for Condensed Matter Physics, Institute of Physics, Chinese Academy of Sciences, Beijing 100190, China
[c] School of Physics, University of Chinese Academy of Sciences, Beijing 100190, China
[d] Materials Research Lab at Songshan Lake, Dongguan 523808, China

ARTICLE INFO

Keywords:
High-pressure synthesis
Quasi-one-dimension
Semiconductor
Magnetism

ABSTRACT

Two quasi-one-dimensional compounds $Ba_9Nb_{2.54}Te_{15}$ and $Ba_9Ta_{1.89}Te_{15}$ were synthesized under high pressure and high temperature conditions and systematically characterized by structural, transport and magnetic measurements. Both the two compounds crystallize into a hexagonal structure with the space group *P*-6*c*2 (No. 188). The structure consists of trimeric face-sharing octahedral $Nb/TaTe_6$ chains separated by a large distance (>10 Å), thus presenting a strong one-dimensional crystal structure. The transport properties suggest that both the two compounds are semiconductors with a band gap ~ 0.15 eV for $Ba_9Nb_{2.54}Te_{15}$ and ~ 0.22 eV for $Ba_9Ta_{1.89}Te_{15}$. Magnetic properties characterization indicates that $Ba_9Nb_{2.54}Te_{15}$ displays no long-range-order above 2 K, but with an effective moment μ_{eff} ~ 1.8 μ_B/f.u., while $Ba_9Ta_{1.89}Te_{15}$ exhibits a diamagnetic behavior. Our results demonstrate that, in the sequence of $Ba_9V_3Te_{15}$, $Ba_9Nb_{2.54}Te_{15}$ and $Ba_9Ta_{1.89}Te_{15}$, the occupation in the transition metal sites decreases, the semiconducting band gap increases, and the magnetism changes from ferromagnetism to diamagnetism.

1. Introduction

Quasi-one-dimensional (1D) systems exhibit plenty of novel physical phenomena arising from their unique low-dimensional structure, such as Tomonaga-Luttinger liquid, spin-Peierls transition and unconventional superconductivity [1–6]. Although an ideal 1D spin chain cannot form a long-range magnetic order at finite temperature, the weak interchain coupling generally gives rise to various and novel magnetic ground states. Recently, a series of ternary compounds RE_3MX_5 (*RE* = Ba or La; *M* = transition metal; *X* = chalcogen or pnicogen) with a Hf_5Sn_3Cu-anti-type structure have been synthesized and actively studied as one of the most typical quasi-1D systems [7–13]. In these compounds, the crystal structure consists of infinite face-sharing octahedral MX_6 chains and *X* chains along the *c* axis, which are separated by Ba or La atoms, thus exhibiting a strong quasi-one-dimensional crystal structure. Several interesting physical properties associated with their quasi-1D crystal structure are reported. For example, La_3MnAs_5 displays a ferromagnetic metal behavior with ferromagnetic transition temperature T_C ~ 112 K, resulting from the orbital hybridization between the $MnAs_6$ chains and intermediate La atom by the itinerant electrons [14]. Its sister compound La_3CrAs_5 also exhibits a ferromagnetic behavior at ~50 K owing to a weaker interchain interaction compared with La_3MnAs_5 [15]. Furthermore, Ba_3TiTe_5 is a typical 1D conductor, exhibiting semiconducting behavior due to Umklapp scatting. The novel properties such as spin density wave/charge density wave (SDW/CDW), and non-Fermi liquid would be suppressed and then superconductivity appears, when the interchain hopping is tuned by external pressure [16]. Specifically, due to the dimerization or trimerization, Ba_3MX_5 shows complex geometric modulated spin interactions, and then presents fantastic physical properties [17–20]. For example, previous study shows that dimerized $Ba_6Cr_2S_{10}$ exhibits a rare ferrotoroidicity with 1D spin chain [17] and trimerized $Ba_9V_3Se_{15}$ exhibits a ferromagnetic transition at 2.5 K and 1D ferromagnetic chains properties, i.e, $T^{1/2}$ dependence of magnetic specific heat above the ordered temperature

* Corresponding authors at: Beijing National Laboratory for Condensed Matter Physics, Institute of Physics, Chinese Academy of Sciences, Beijing 100190, China.
E-mail addresses: zhang@iphy.ac.cn (J. Zhang), wangxiancheng@iphy.ac.cn (X. Wang), jin@iphy.ac.cn (C. Jin).

https://doi.org/10.1016/j.jallcom.2024.176496
Received 3 July 2024; Received in revised form 26 August 2024; Accepted 12 September 2024
Available online 13 September 2024

[19].

Very recently, the quasi-1D compound $Ba_9V_3Te_{15}$ was synthesized and systematic physical properties measurements were carried out. $Ba_9V_3Te_{15}$ undergoes a ferromagnetic semiconductor behavior with $T_c \sim 3.5$ K and band gap ~0.128 eV, and the short-range spin orders arising from the intrachain spin coupling result in a negative magnetoresistance effect [21]. Although a large numbers of compounds Ba_3MX_5 are synthesized and studied in succession, the *M* ions generally are limited to 3*d* transition metal element in the series of Ba_3MX_5 except $Ba_9Sn_3Te_{15}$ and $Ba_9Sn_3Se_{15}$.[22] It is known that compared with that in 3*d*-orditals, the electrons in 4*d*- and 5*d*-orditals tend to be more delocalized. When *M* ions are replaced by 4*d*- or 5*d*- transition metal element, it possibly causes a significant influence on the physical properties of Ba_3MX_5 and thus it is interesting to study the evolution of their physical properties with *M* ions varying from 3*d*- to 5*d*-elements.

In this paper, we have set out to conduct an exploratory work to replace V ions by other homologous main group elements and successfully prepared two quasi-1D compounds $Ba_9Nb_{2.54}Te_{15}$ and $Ba_9Ta_{1.89}Te_{15}$. Herein, we reported on the synthesis and evolution of structure and physical properties of the two compounds in comparison with their sister compound $Ba_9V_3Te_{15}$.

2. Experimental

The synthesis of $Ba_9M_3Te_{15}$ (M = Nb, Ta) was performed under high pressure and high temperature conditions using a DS 6 × 800 T cubic anvil high-pressure apparatus. Commercially available lumps of Ba (Alfa, immersed in oil, >99.2 % pure) and crystalline powders of Nb (Alfa, 99.99 % pure), Ta (Alfa 99.99 % pure) and Te (Alfa, 99.999 % pure) were used as the starting materials. The precursor BaTe was prepared by the reaction of the Ba lumps and Te powders in an evacuated quartz tube at 600 ℃ for 10 h. The mixture of BaTe, *M* (M = Nb, Ta), and Te powders with a stoichiometric proportion of 3:1:2 was finely ground and pressed into a pellet with a diameter of 6 mm, which then was sintered at 1200 ℃ and 5.5 GPa for 30 min. The pressure was released after the temperature was quenched to room temperature, and finally the black polycrystalline samples of $Ba_9M_3Te_{15}$ were obtained. Furthermore, we also tried to synthesize $Ba_9M_3Te_{15}$ at ambient pressure by heating the mixture of Ba lumps, Nb or Ta powders and Te powders with a stoichiometric radio of 3:1:5 at 1200 ℃ for 24 h. However, we cannot obtain the samples of $Ba_9M_3Te_{15}$ except BaTe and some unknow impurities via ambient synthesis, which indicates that it is necessary to prepare $Ba_9M_3Te_{15}$ under high pressure and high temperature conditions.

Powder X-ray diffraction (XRD) measurement was carried out on a Rigaku Ultima VI (3 kW) diffractometer using Cu K_α radiation (λ = 1.54060 Å), which is generated at 40 kV and 40 mA. The data was collected with a scanning rate of 1° per minute and a scanning step length of 0.02 degree. The Rietveld refinements on the diffraction patterns were carried out using the GSAS software package. Energy dispersive x-ray spectroscopy (EDX) was measured to confirm the chemical composition of the two compounds $Ba_9M_3Te_{15}$ (M = Nb, Ta). The temperature dependence of electrical resistivity ρ(T) was measured by four-probe electrical conductivity methods from 2 to 300 K in physical properties measuring system (PPMS). Furthermore, specific heat was also measured in the temperature range of 2 – 40 K using PPMS. The *dc* magnetic susceptibility(χ) measurement was carried out using a superconducting quantum interference device (SQUID-VSM; Quantum Design) in the temperature range of 2–300 K.

3. Results and discussions

Two new compounds $Ba_9M_3Te_{15}$ (M = Nb, Ta) were prepared under high-pressure and high-temperature conditions. The chemical compositions of them were determined by EDX and the results are shown in Fig. 1(a) and (b). EDX measurements were carried out on the surface of

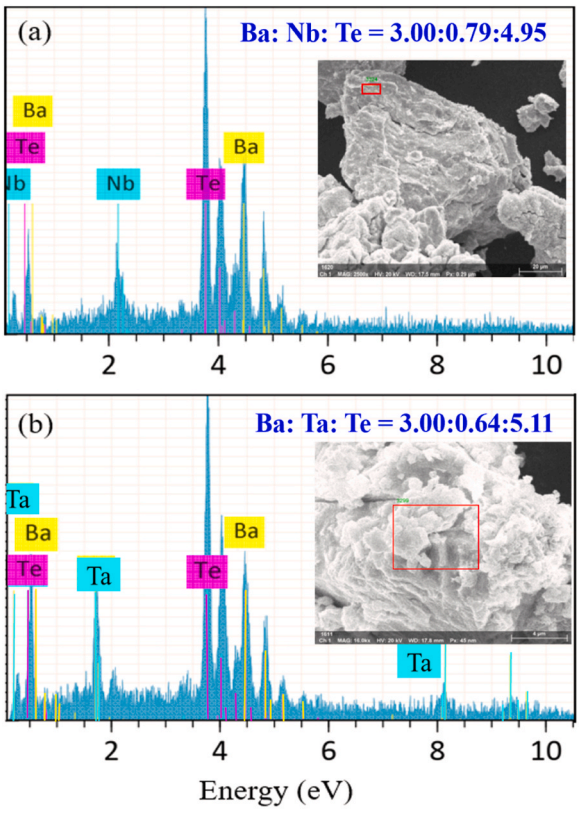

Fig. 1. Energy dispersive x-ray spectrum of (a) $Ba_9Nb_3Te_{15}$ and (b) $Ba_9Ta_3Te_{15}$.

the two compounds at several different areas, as shown in the inset of Fig. 1(a) and (b). The average atomic ratios of Ba: *M*: Te can be calculated to be about 3.00: 0.79: 4.95 for $Ba_9Nb_3Te_{15}$ and 3.00: 0.64: 5.11 for $Ba_9Ta_3Te_{15}$. The occupancy of transition metal ions *M* is obviously smaller than the stoichiometric ratio of $Ba_9M_3Te_{15}$, which indicates that there occur some vacancies in the transition metal *M* sites of the two compounds.

Fig. 2(a) and (b) shows the powder XRD patterns measured at room temperature of $Ba_9Nb_3Te_{15}$ and $Ba_9Ta_3Te_{15}$, respectively. All the peaks can be indexed by a hexagonal structure with the lattice parameters of $a = b = 10.204(1)$ Å and $c = 20.058(7)$ Å for $Ba_9Nb_3Te_{15}$, and $a = b = 10.160(6)$ Å and $c = 20.141(7)$ Å for $Ba_9Ta_3Te_{15}$. The similar compounds have been reported to generally undergo a trimerized structure with the space group of *P*-6*c*2 (No. 188), for example, single crystals of $Ba_9Fe_3Se_{15}$ [19], $Ba_9Sn_3Te_{15}$ [22] and $Ba_9V_3S_{15}$ [23], and polycrystalline samples of $Ba_9Fe_3Te_{15}$ [9], $Ba_9V_3Se_{15}$ [20] and $Ba_9V_3Te_{15}$ [21]. Hence, the crystal structure of very recently discovered $Ba_9V_3Te_{15}$ with the space group of *P*-6*c*2 (No. 188) could be adopted as the initial model to refine the diffraction data of $Ba_9M_3Te_{15}$ (M = Nb, Ta) [21]. By using GSAS software packages, the refinements were conducted and smoothly converged to $\chi^2 = 2.38$, $R_{wp} = 3.47$ %, $R_p = 2.60$ % for $Ba_9Nb_3Te_{15}$ and $\chi^2 = 3.59$, $R_{wp} = 4.63$ %, $R_p = 3.89$ % for $Ba_9Ta_3Te_{15}$. The summary of the crystallographic data is listed in Table 1. Some selected important distances and angles between atoms are summarized in Table 2. For comparing, the lattice parameters and selected distances of their sister compound $Ba_9V_3Te_{15}$ are listed in Table 2 as well. It is evident that there are some vacancies in the Nb and Ta sites of the two compounds. The total vacancies in the Nb/Ta sites can be calculated to be 0.46 for $Ba_9Nb_3Te_{15}$ and ~1.11 for $Ba_9Ta_3Te_{15}$, which are very close to the obtained results measured by EDX, indicating that the chemical formula should be changed to $Ba_9Nb_{2.54}Te_{15}$ and $Ba_9Ta_{1.89}Te_{15}$. The similar situation has been observed in the series of $Ba_9Sn_3(Te_{1-x}Se_x)_{15}$ with the vacancies in the Sn site [22]. It seems that the vacancies in the transition metal sites gradually become larger in the sequence of

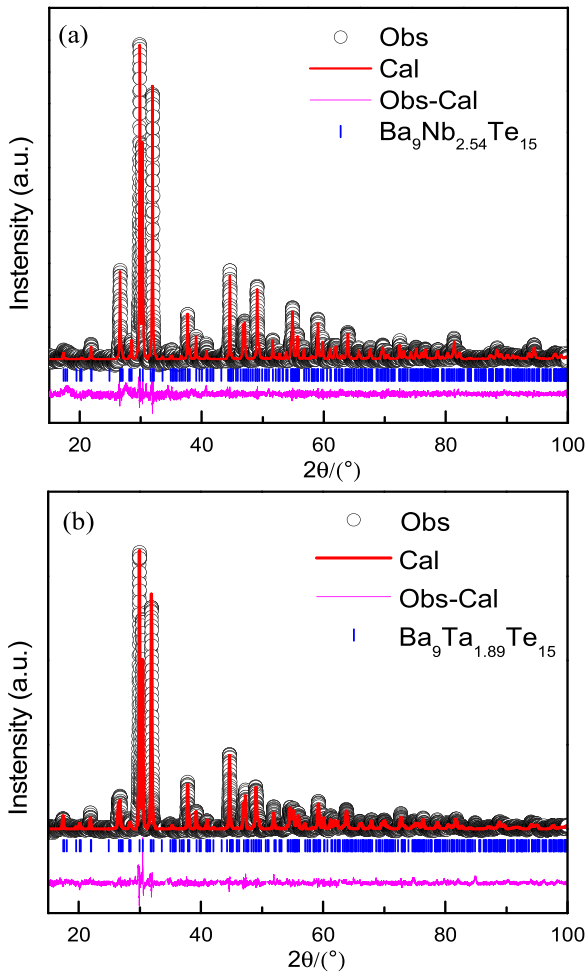

Fig. 2. Powder XRD patterns of (a) $Ba_9Nb_{2.54}Te_{15}$ and (b) $Ba_9Ta_{1.89}Te_{15}$ measured at 300 K and the refinement with the space group of *P*-6*c*2 (No. 188).

$Ba_9V_3Te_{15}$, $Ba_9Nb_{2.54}Te_{15}$ and $Ba_9Ta_{1.89}Te_{15}$.

Fig. 3 shows the sketch of the crystal structure of $Ba_9Nb_{2.54}Te_{15}$ and $Ba_9Ta_{1.89}Te_{15}$. The top view with the projection along the *c* axis and the perspective view with the projection along the [*110*] direction is drawn in Figs. 3(a) and 3(b), respectively. The structure consists of infinite face-sharing octahedral MTe_6 (M = Nb, Ta) chains along the *c* axis, which are arranged in a triangular lattice form and separated by Ba and Te atoms with a large distance (> 10 Å), demonstrating a strong 1D structure character. As shown in Fig. 3(c), there are two Wyckoff positions for *M* atoms: *M*1 at (0, 0, 0) and *M*2 at (0, 0, *z*), which results in a trimerized structure feature. Each *M* ion is surround by six Te ions to form face-sharing MTe_6 octahedron chains. In the MTe_6 chains, the distances between adjacent *M* atoms are 3.107(1) Å and 3.815(2) Å for $Ba_9Nb_{2.54}Te_{15}$, and 3.168(3) Å and 3.734(3) Å for $Ba_9Ta_{1.89}Te_{15}$. When the V ions are replaced by Nb ions, both the lattice parameters a = 10.204(1) Å and c = 20.058(7) Å of $Ba_9Nb_{2.54}Te_{15}$ are larger than those of $Ba_9V_3Te_{15}$, because of the larger ionic radius of Nb ions relative to V ions. For $Ba_9Ta_{1.89}Te_{15}$, the lattice parameter a = 10.160(5) Å is smaller but the c = 20.141(7) Å is larger than that of $Ba_9Nb_{2.54}Te_{15}$. The decrease of the lattice parameter *a* might be mainly caused by the large vacancies in the Ta sites. The bond angles ∠Te-*M*-Te in MTe_6 octahedron, as shown in Fig. 3(c), are listed in Table 2. It is observed that the bond angels α of Te1-*M*1-Te1 in the $M1Te_6$ octahedron are 179.7(6)° for $Ba_9Nb_{2.54}Te_{15}$ and 179.8(3)° for $Ba_9Ta_{1.89}Te_{15}$, suggesting the distorted degree of $M1Te_6$ octahedron is very close. However, in the $M2Te_6$ octahedron, the bond angles β of Te1-*M*2-Te2 are 170.9(3)° for $Ba_9Nb_{2.54}Te_{15}$ and 175.6(0)° for $Ba_9Ta_{1.89}Te_{15}$, respectively. These

Table 1
The summary of crystallographic data at room-temperature for $Ba_9Nb_{2.54}Te_{15}$ [a] and $Ba_9Ta_{1.89}Te_{15}$ [b], respectively.

site	Wyck	*x/a*	*y/b*	*z/c*	*Occ*	U_{iso} (Å)
$Ba_9Nb_{2.54}Te_{15}$						
Ba1	12 l	0.0029(2)	0.3756(7)	0.0801(5)	1	0.020(4)
Ba2	6k	0.4054(0)	0.3784(1)	0.25	1	0.021(3)
Nb1	2a	0	0	0	0.88 (3)	0.015(3)
Nb2	4 g	0	0	0.1549(1)	0.83(0)	0.024(6)
Te1	12 l	0.2440(2)	0.2434(2)	0.0826(5)	1	0.014(4)
Te2	6k	−0.0007(8)	0.2280(1)	0.25	1	0.036(5)
Te3	2c	0.3333(3)	0.6666(7)	0	1	0.008(5)
Te4	4 h	0.3333(3)	0.6666(7)	0.1741(7)	1	0.001(5)
Te5	4i	0.6666(7)	0.3333(3)	0.1595(1)	1	0.025(1)
Te6	4i	0.6666(7)	0.3333(3)	0.0228(1)	0.5	0.003(0)
$Ba_9Ta_{1.89}Te_{15}$						
Ba1	12 l	0.0175(1)	0.3934(3)	0.0842(6)	1	0.035(7)
Ba2	6k	0.3795(8)	0.3713(5)	0.25	1	0.009(3)
Ta1	2a	0	0	0	0.53(0)	0.013(4)
Ta2	4 g	0	0	0.1573(2)	0.68(5)	0.010(8)
Te1	12 l	0.2316(7)	0.2311(7)	0.0833(2)	1	0.034(4)
Te2	6k	0.0022(1)	0.2470(6)	0.25	1	0.027(5)
Te3	2c	0.33333	0.66667	0	1	0.023(4)
Te4	4 h	0.33333	0.66667	0.1703(9)	1	0.025(7)
Te5	4i	0.66667	0.33333	0.1632(6)	1	0.023(9)
Te6	4i	0.66667	0.33333	0.0078(3)	0.5	0.019(6)

[a] Crystal data: space group *P*-6*c*2 (No.188) $a = b$ = 10.204(1) Å, c = 20.058(7) Å, Z = 2, V = 1808.75(4) Å^3, χ^2 = 2.38, R_p = 2.60 %, R_{wp} = 3.47 %
[b] Crystal data: space group *P*-6*c*2 (No.188) $a = b$ = 10.160(6) Å, c = 20.141(7) Å, Z = 2, V = 1800.8(2) Å^3, χ^2 = 3.59; R_p = 3.89 %, R_{wp} = 4.63 %

Table 2
The lattice parameter (Å) and selected interatomic distances (Å) and angles (°) in $Ba_9V_3Te_{15}$, $Ba_9Nb_{2.54}Te_{15}$ and $Ba_9Ta_{1.89}Te_{15}$. (a) the data is from ref [21].

Compounds	[(a)]$Ba_9V_3Te_{15}$	$Ba_9Nb_{2.54}Te_{15}$	$Ba_9Ta_{1.89}Te_{15}$
a	10.184(8)	10.204(1)	10.160(7)
c	19.948(7)	20.058(7)	20.141(8)
*M*1 - *M*2	3.233(3)	3.107(1)	3.168(3)
*M*2 - *M*2	3.507 (7)	3.815(2)	3.733(5)
*M*1-Te1	2.938(7)	2.987(7)	2.888(8)
*M*2-Te1	2.860(6)	2.878(3)	2.784(1)
*M*2-Te2	2.862(1)	3.011(4)	3.119(1)
Te3 - Te4	3.379(7)	3.492(2)	3.432(1)
Te4 - Te4	3.215(1)	3.044(9)	3.206(6)
Te5 - Te6	2.915(1)	2.742(0)	3.132(2)
Te5 – Te5	3.43(4)	3.630(6)	3.492(6)
∠Te1-*M*1-Te1	178.8(2)	179.7(6)	179.8(3)
∠Te1-*M*2-Te2	174.8(6)	170.9(3)	175.6(0)

results indicate that the $Nb2Te_6$ octahedron in $Ba_9Nb_{2.54}Te_{15}$ is more compressed than $Ta2Te_6$ octahedron of $Ba_9Ta_{1.89}Te_{15}$. In other words, the $TaTe_6$ octahedral chain in $Ba_9Ta_{1.89}Te_{15}$ is more stretched along the *c* axis than that of $Ba_9Nb_{2.54}Te_{15}$ and thus leads to the increase of the lattice parameter *c*. However, the crystal volume of $Ba_9Ta_{1.89}Te_{15}$ is obviously smaller than that of $Ba_9Nb_{2.54}Te_{15}$, which should be attributed to the large vacancies in the Ta sites.

Besides the MTe_6 chains, there are two Te chains located in the center of the triangular lattices, that is the (1/3, 2/3, *x*) and (2/3, 1/3, *y*) sites, also shown in Fig. 3(c). In addition, for the sites occupied by the Te6 atoms, the occupation ratio is 0.5. The distances of the adjacent Te atoms in the Te chains range from 2.742(0) Å to 3.630(6) Å for $Ba_9Nb_{2.54}Te_{15}$ and from 3.132(2) Å to 3.492(6) Å for $Ba_9Ta_{1.89}Te_{15}$. The Te4-Te4 and Te5-Te6 distances in $Ba_9Nb_{2.54}Te_{15}$ and $Ba_9Ta_{1.89}Te_{15}$ are comparable with that in the typical bond length of Te-Te (~2.8 Å) [24], which implies that the Te_2^{2-} dimer is formed and partial covalent bonds exist in the Te chains. The similar Te_2^{2-} dimer has also been reported in iso-structure compounds $Ba_9V_3Te_{15}$ [21] and $Ba_9Sn_3Te_{15}$ [22]. Hence, the chemical formula of $Ba_9[Nb_{2.54}/Ta_{1.89}]Te_{15}$ can be rewritten as $Ba_9[Nb_{2.54}/Ta_{1.89}]$ $(Te^{2-})_9[(Te^{2-})_2(Te_2^{2-})_2]$ like their sister compound

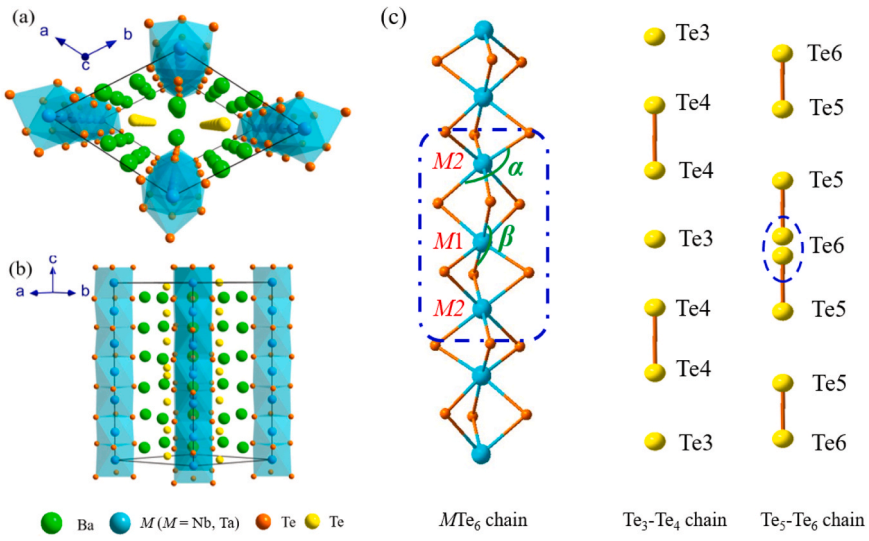

Fig. 3. The sketch of the crystal structure of $Ba_9Nb_{2.54}Te_{15}$ and $Ba_9Ta_{1.89}Te_{15}$: (a) the view along the *c* axis direction showing the hexagonal geometry arrangement; (b) the view from the [110] projection. (c) The sketch of MTe_6 octahedral chains and Te chains in the compounds of $Ba_9Nb_{2.54}Te_{15}$ and $Ba_9Ta_{1.89}Te_{15}$.

$Ba_9V_3Te_{15}$, and the total valence state of transition metal *M* should be +8 considering the charge balance. For $Ba_9V_3Te_{15}$, the valence states of V1 and V2 are speculated to be +2 and +3, respectively, and the total charges of the three V ions are exactly 8 [21]. It is known that the electronegativity of the transition metal gradually decreases in the sequence of V, Nb and Ta, which indicates that Nb and Ta ions tend to form higher valence state relative to V ions, for example, the common valences of Ta ions are +4 and +5. Based on the Bond Valence Sum Rule, the valence state *V* can be obtained by the formula $V = \sum e^{((r_0-r)/b)}$, where $r_0 \sim 2.70$ is the empirical distance for Nb-Te and Ta-Te pairs, $b = 0.37$ is the universal parameter and *r* is the *M*-Te bond length in MTe_6 octahedron obtained by the refinements. The calculated valence states are ~2.76 for Nb, ~ 3.15 for Nb2, ~3.60 for Ta1 and ~3.68 for Ta2, which indicates that the valence states are +3 for Nb ions and +4 for Ta ions. As expected, compared with $Ba_9V_3Te_{15}$, the valence states of *M* ions increase with *M* ions varying from V to Ta. However, if the Nb and Ta sites are fully occupied in $Ba_9M_3Te_{15}$ (*M* = Nb, Ta), the total charges of Nb and Ta would be larger than +8. Therefore, there should be vacancies exist in the Nb and Ta sites, and the factual chemical formula should be $Ba_9Nb_{2.66}Te_{15}$ and $Ba_9Ta_2Te_{15}$ based on the charge balance, agreed with the results of our Rietveld refinements and EDX measurements. Furthermore, the degree of trimerization is defined as the ratio of $|d - d_{intra}|/|d_{inter} + d_{intra}|$, where d_{inter} is the distance of the adjacent *M*2 ions and d_{intra} is that of the adjacent *M*1 and *M*2 ions. [21] The calculated values of trimerization degree are 0.0407, 0.1139 and 0.0820 for the three compounds $Ba_9V_3Te_{15}$, $Ba_9Nb_{2.54}Te_{15}$ and $Ba_9Ta_{1.89}Te_{15}$, respectively. $Ba_9Nb_{2.54}Te_{15}$ has the largest trimerization degree value, which might be due to its moderate electronegativity and vacancies in the Nb sites.

Fig. 4 exhibits the electronic resistivity dependent on temperature for $Ba_9V_3Te_{15}$, $Ba_9Nb_{2.54}Te_{15}$ and $Ba_9Ta_{1.89}Te_{15}$ samples. For comparing, the resistivity of the sister compound $Ba_9V_3Te_{15}$ is also shown in Fig. 4. The resistivity is approximate 1.14 Ω-cm for $Ba_9Nb_{2.54}Te_{15}$ and 7.68 Ω-cm for $Ba_9Ta_{1.89}Te_{15}$ at room temperature. As the temperature decreases, the resistivity gradually increases, which demonstrates a typical semiconducting behavior. Furthermore, the plots of lnρ versus $1/T$ are exhibited in the inset of Fig. 4. It can be seen that the curves of lnρ ($1/T$) exhibit a nearly straight line in the whole measured temperature range, indicating that the Arrhenius law for thermally activated conduction is able to be used to describe the semiconducting behavior of the three compounds. We used the formula $\rho \propto \exp(\Delta_g/2k_BT)$, where Δ_g is the semiconducting band gap and k_B is the Boltzman's constant, to fit the resistivity curves, as shown in the inset of Fig. 4. These resistivity curves

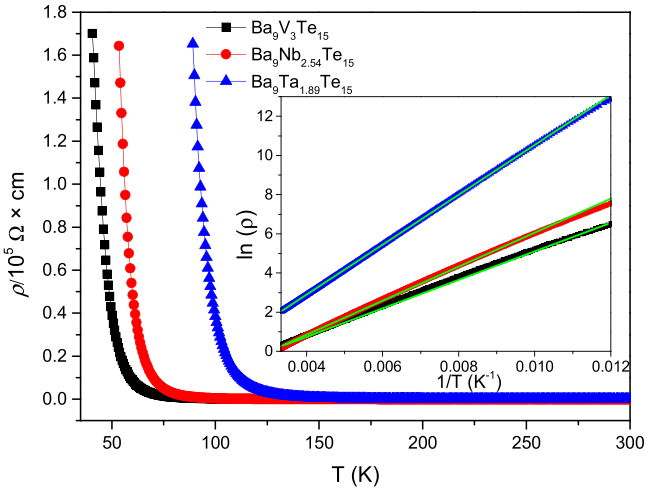

Fig. 4. The temperature dependence of resistivity for $Ba_9V_3Te_{15}$, $Ba_9Nb_{2.54}Te_{15}$ and $Ba_9Ta_{1.89}Te_{15}$. The inset shows lnρ versus $1/T$ and the green lines are the linear fitting in the whole measured temperature region.

can be well fitted and results in band gap Δ_g to be 0.15 eV for $Ba_9Nb_{2.54}Te_{15}$ and 0.22 eV for $Ba_9Ta_{1.89}Te_{15}$. The evolution of transport properties for the three compounds $Ba_9V_3Te_{15}$, $Ba_9Nb_{2.54}Te_{15}$ and $Ba_9Ta_{1.89}Te_{15}$ will be discussed latter.

Fig. 5(a) shows the magnetic susceptibility $\chi(T)$ as a function of temperature of $Ba_9Nb_{2.54}Te_{15}$, measured under the field of 1000 Oe in both the field-cooling (FC) and zero-field-cooling (ZFC) models. The ZFC and FC curves are overlapped in the whole temperature range and the magnetic susceptibility gradually increases with the decrease of temperature and displays an upturn at the low temperature, demonstrating a paramagnetic-like behavior. Then the modified Curie-Weiss law $\chi = \chi_0 + C/(T\text{-}T_\theta)$, where χ_0 is the susceptibility independent of temperature, *C* is the Curie constant and T_θ is the Weiss temperature, was used to fit the susceptibility in the high temperature region between 100 K and 300 K. After the fitting, the values of χ_0, Weiss temperature T_θ and Curie constant *C* can be obtained to be -7.21×10^{-4} emu/mol-Oe, −48.9 K and 0.405 emu-K/mol-Oe, respectively. The inverse susceptibility $1/(\chi\text{-}\chi_0)$ (T) is also shown in the Fig. 5(a). The negative value of T_θ indicates that the anti-ferromagnetic interaction plays a dominated role in $Ba_9Nb_{2.54}Te_{15}$. Furthermore, according to the formula $\mu_{eff} = \sqrt{8C}$, the

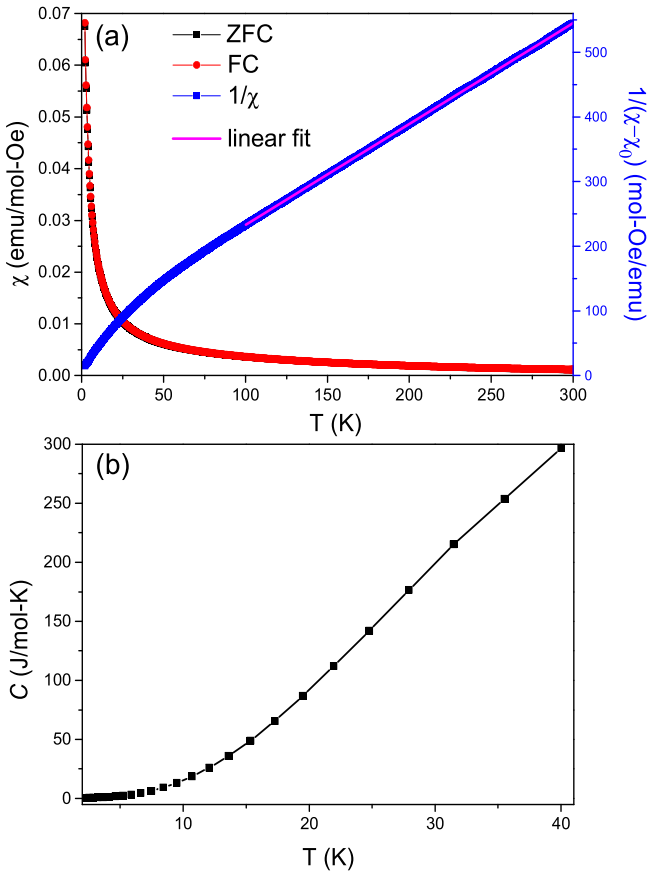

Fig. 5. (a) The magnetic susceptibility $\chi(T)$ as a function of temperature for $Ba_9Nb_{2.54}Te_{15}$. The inverse susceptibility $1/(\chi\text{-}\chi_0)$ (T) for $Ba_9Nb_{2.54}Te_{15}$ is shown in right axis. The purple line is the fit of modified Curie-Weiss law between 100 and 300 K. (b) Temperature-dependent specific heat between 2 and 40 K for $Ba_9Nb_{2.54}Te_{15}$.

effective moment μ_{eff} is estimated to be 1.8 μ_B /f.u, corresponding to the local spin $S = 0.5/2$ per Nb ions, while the theoretical value of the effective moment of $Ba_9Nb_{2.54}Te_{15}$ with Nb^{3+} ions is calculated to be $g\mu_B\sqrt{\frac{2}{2}\times(\frac{2}{2}+1)\times 2.54} \approx 4.5$ μ_B/f.u., where the Lande factor g is assigned to be 2. It can be seen that the effective moment μ_{eff} obtained from our magnetic susceptibility measurements is much smaller than the theoretical value of the effective moment. We speculate that the 4*d* electrons of Nb atoms are more delocalized and then results in the reduction of the effective moment μ_{eff} for $Ba_9Nb_{2.54}Te_{15}$. Furthermore, the temperature dependence of specific heat $C(T)$ for $Ba_9Nb_{2.54}Te_{15}$ was measured within the temperature range from 2 K and 40 K, as shown in Fig. 5(b). It is observed that there is no noticeable anomaly in the whole measured temperature range, which confirms that no long-range order occurs above 2 K for $Ba_9Nb_{2.54}Te_{15}$ in agreement with the magnetic susceptibility measurements.

The temperature dependence of magnetic susceptibility $\chi(T)$ for $Ba_9Ta_{1.89}Te_{15}$ is shown in Fig. 6. We can see that the FC and ZFC curves are also overlapped in the whole temperature range, demonstrating a paramagnetic-like behavior, which is similar with that of $Ba_9Nb_{2.54}Te_{15}$. However, the magnetic susceptivity in the high temperature region, as shown in the inset of Fig. 6, is negative. These results indicate that $Ba_9Ta_{1.89}Te_{15}$ exhibits a diamagnetic behavior and the upturn of $\chi(T)$ at low temperature, which may be related to the paramagnetic impurities, possible unknown tantalum compounds formed by the excess Ta atoms owing to the vacancies in the Ta sites.

In the series of $Ba_9V_3Te_{15}$, $Ba_9Nb_{2.54}Te_{15}$ and $Ba_9Ta_{1.89}Te_{15}$, it is reported that $Ba_9V_3Te_{15}$ undergoes a ferromagnetic behavior with a

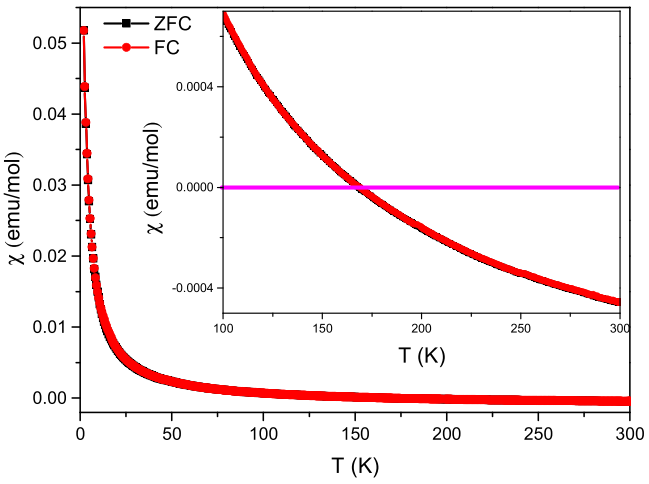

Fig. 6. Temperature dependence of magnetic susceptibility $\chi(T)$ for $Ba_9Ta_{1.89}Te_{15}$. The inset shows the enlarge of the high temperature region.

ferromagnetic transition temperature $T_c \sim 3.6$ K and the effective moment $\mu_{eff} \sim 5.87$ μ_B /f.u. However, no long-range order above 2 K is observed in $Ba_9Nb_{2.54}Te_{15}$ and the effective moment μ_{eff} is reduced to ~1.8 μ_B /f.u. For the $Ba_9Ta_{1.89}Te_{15}$ sample, it presents a diamagnetic behavior. The larger number of vacancies in the Ta sites indicate that the valence states of Ta ions are higher than that of Nb ions, and it is known that the electrons in higher *d* orbital generally tend to be delocalized, which causes that in the sequence of $Ba_9V_3Te_{15}$, $Ba_9Nb_{2.54}Te_{15}$ and $Ba_9Ta_{1.89}Te_{15}$, the effective moment μ_{eff} related to the local moment becomes smaller and to zero in the case of $Ba_9Ta_{1.89}Te_{15}$. The diamagnetic behavior has also been observed in other Ta-based compounds, such as TaAs [25]. The electrical band structure calculations, without including spin orbital coupling (SOC), suggest that TaAs should be a metal and the bands near the Fermi energy are mainly formed by Ta 5*d* orbitals. While small band gaps are opened when the SOC is included in the calculations, indicating a Weyl semimetal nature for TaAs [26,27]. It has been speculated that TaAs is a Landau diamagnetism, which arises from the linearly dispersed bands [28]. Here, the origin of diamagnetism in $Ba_9Ta_{1.89}Te_{15}$ is deserved to be studied in the future.

In transport properties, $Ba_9V_3Te_{15}$ is reported to be a semiconductor with a band gap 0.128 eV, and both $Ba_9Nb_{2.54}Te_{15}$ and $Ba_9Ta_{1.89}Te_{15}$ also display a semiconducting behavior, as shown in Fig. 3. It can be seen that the band gap gradually increases from $Ba_9V_3Te_{15}$ to $Ba_9Ta_{1.89}Te_{15}$. It has been reported that for $Ba_9V_3Te_{15}$ the trimerization of Te chains plays a key role in opening a gap and then leading to the semiconducting behavior [21]. Among the three compounds of $Ba_9V_3Te_{15}$, $Ba_9Nb_{2.54}Te_{15}$ and $Ba_9Ta_{1.89}Te_{15}$, $Ba_9Nb_{2.54}Te_{15}$ has the largest trimerization degree. The larger band gap in $Ba_9Nb_{2.54}Te_{15}$ relative to $Ba_9V_3Te_{15}$ suggests that the distortion of Te chains should dominate the semiconducting behavior in $Ba_9Nb_{2.54}Te_{15}$. Furthermore, the disorder caused by the vacancies also makes an important contribution in the semiconducting behavior. It is speculated that the partial delocalized *d* electrons are shared within the trimmer unit and lose their local spin moments, while the hopping between trimmer units for these *d* electrons might be limited owing to the disorder caused by the vacancies. Therefore, for $Ba_9Ta_{1.89}Te_{15}$, there are a lot of vacancies in the Ta sites, and the disorder-induced localization between the trimmer units is speculated to mainly contribute to the semiconducting behavior and produce the largest band gap.

4. Conclusions

The two compounds $Ba_9Nb_{2.54}Te_{15}$ and $Ba_9Ta_{1.89}Te_{15}$ with trimeric face-sharing octahedral MTe_6 chains were successfully synthesized under high pressure and high temperature conditions. These compounds

crystalize into a hexagonal structure with space group *P*-6*c*2 (No. 188) and some vacancies occur in the transition metal *M* sites. In transport properties, they both exhibit a semiconducting behavior with the band gap ~0.15 eV for $Ba_9Nb_{2.54}Te_{15}$ and ~0.22 eV for $Ba_9Ta_{1.89}Te_{15}$. Magnetic measurements reveal that although there is an effective moment μ_{eff} ~1.8 μ_B/f.u., no long-rage order above 2 K occurs in $Ba_9Nb_{2.54}Te_{15}$, while the diamagnetism is found at high temperature region in $Ba_9Ta_{1.89}Te_{15}$. In comparison with $Ba_9V_3Te_{15}$, when the ion varies from V to Ta, the electrons from 3*d*- to 5*d*- orbitals tend to delocalized, which is speculated to lead to the evolution of the magnetic properties. Furthermore, the largest trimerization degree for $Ba_9Nb_{2.54}Te_{15}$ results in the larger band gap compared with $Ba_9V_3Te_{15}$, while $Ba_9Ta_{1.89}Te_{15}$ undergoes the largest band gap, which possibly results from the numerous vacancies in the Ta sites.

CRediT authorship contribution statement

Xiaoming Chen: Investigation, Formal analysis, Data curation. **Zhiwei Zhao:** Visualization, Supervision. **Changjiang Xiao:** Writing – original draft, Formal analysis. **Xiancheng Wang:** Writing – review & editing, Writing – original draft, Supervision, Methodology. **Lei Duan:** Writing – review & editing, Writing – original draft, Visualization, Supervision, Investigation, Formal analysis, Data curation. **Changqing Jin:** Writing – original draft, Visualization, Supervision, Methodology. **Jun Zhang:** Visualization, Supervision, Methodology. **Yagang Feng:** Visualization, Formal analysis. **Shun Wang:** Visualization, Formal analysis. **Suxuan Du:** Validation, Data curation. **Zelong Wang:** Formal analysis, Data curation. **Yanteng Wei:** Investigation, Formal analysis, Data curation.

Declaration of Competing Interest

The authors declare that they have no known competing financial interests or personal relationships that could have appeared to influence the work reported in this paper.

Data Availability

Data will be made available on request.

Acknowledgments

This work was supported by National Key R&D Program of China under Grant No. 2023YFA1406001, National Natural Science Foundation of China under Grants No. 12104488 & 12404005 and China Postdoctoral Science Foundation under Grant No. 2023M741036. We also appreciate the support by Key R & D projects of Henan Province under Grant No. 221111230800 and Key Scientific and Technological Research Projects in Henan Province under Grant No. 242102231068.

References

[1] Q. Faure, S. Takayoshi, V. Simonet, B. Grenier, M. Mansson, J.S. White, G. S. Tucker, C. Ruegg, P. Lejay, T. Giamarchi, S. Petit, Tomonaga-Luttinger liquid spin dynamics in the quasi-one-dimensional Ising-like antiferromagnet $BaCo_2V_2O_8$, Phys. Rev. Lett. 123 (2) (2019) 027204.

[2] M. Nakamura, A. Sekiyama, H. Namatame, A. Fujimori, H. Yoshihara, T. Ohtani, A. Misu, M. Takano, Metal-semiconductor transition and Luttinger-liquid behavior in quasi-one-dimensional $BaVS_3$ studied by photoemission spectroscopy, Phys. Rev. B. 49 (1994) 16191.

[3] A.I. Buzdin, L. Bulaevskii, Spin-Peierls transition in quasi-one-dimensional crystals, Sov. Phys. Usp. 23 (1980) 209.

[4] J.M. Law, C. Hoch, R. Glaum, I. Heinmaa, R. Stern, J. Kang, C. Lee, M.H. Whangbo, R.K. Kremer, Spin-Peierls transition in the $S = 1/2$ compound $TiPO_4$ featuring large intrachain coupling, Phys. Rev. B. 83 (1980) 180414.

[5] J.K. Bao, J.Y. Liu, C.W. Ma, Z.H. Meng, Z.T. Tang, Y.L. Sun, H.F. Zhai, H. Jiang, H. Bai, C.M. Feng, Superconductivity in quasi-one-dimensional $K_2Cr_3As_3$ with significant electroncorrelations, Phys. Rev. X. 5 (2015) 011013.

[6] Z.Y. Liu, Q.X. Dong, P.T. Yang, P.F. Shan, B.S. Wang, J.P. Sun, Z.L. Dun, Y. Uwatoko, G.F. Chen, X.L. Dong, Z.X. Zhao, J.G. Cheng, Pressure-induced superconductivity up to 9 K in the quasi-one-dimensional KMn_6Bi_5, Phys. Rev. Lett.. 128 (2022) 187001.

[7] L. Duan, X.C. Wang, J. Zhang, J.F. Zhao, L.P. Cao, W.M. Li, R.Z. Yu, Z. Deng, C. Q. Jin, Synthesis, structure, and properties of $Ba_9Co_3Se_{15}$ with one-dimensional spin chains, Chin.. Phys. B. 29 (3) (2020) 036102.

[8] B. Almoussawi, H. Tomohiri, H. Kageyama, H. Kabbour, High Pressure Synthesis of the Spin Chain Sulfide $Ba_9V_3S_{11}(S_2)_2$, Eur. J. Inorg. Chem. 13 (2021) 1271–1277.

[9] J. Zhang, L. Duan, Z. Wang, X. Wang, J. Zhao, M. Jin, W. Li, C. Zhang, L. Cao, Z. Deng, The synthesis of a quasi-one-dimensional iron-based telluride with antiferromagnetic chains and a spin glass state, Inorg. Chem. 59 (8) (2020) 5377–5385.

[10] L. Duan, X. Wang, J. Zhang, J. Zhao, Z. Zhao, C. Xiao, C. Guan, S. Wang, L. Shi, J. Zhu, Critical behavior of the ferromagnetic metal La_3CrAs_5 with quasi-one-dimensional spin chains. J. Alloy. Compd. 905 (2022) 164214.

[11] L. Duan, J. Zhang, X. Wang, J. Zhao, L. Cao, W. Li, Z. Deng, R. Yu, Z. Li, C. Jin, High-pressure synthesis, structure and properties of new ternary pnictides La_3TiX_5 (X = P, As), J. Alloy. Compd. 831 (2020) 154697.

[12] L. Duan, Y. Wei, H. Zhang, X. Wang, S. Du, Y. Feng, S. Cai, J. Zhao, J. Zhang, Z. Wang, Suppression of ferromagnetism in La_3CrAs_5 via V substitution, J. Magn.. Magn. Mater. 589 (2024) 171583.

[13] C. Zhang, Y. Wang, J. Zheng, L. Du, Y. Li, X. Han, E. Liu, Q. Wu, Y. Shi, Crystal growth, transport, and magnetic properties of quasi-one-dimensional La_3MnBi_5, Phys. Rev. Mater. 8 (2024) 034402.

[14] L. Duan, X.C. Wang, J. Zhang, Z. Hu, J.F. Zhao, Y.G. Feng, H.L. Zhang, H.J. Lin, C. T. Chen, W. Wu, Synthesis, structure, and magnetism in the ferromagnet La_3MnAs_5: Well-separated spin chains coupled via itinerant electrons, Phys. Rev. B. 106 (2022) 184405.

[15] L. Duan, X. Wang, F. Zhan, J. Zhang, Z. Hu, J. Zhao, W. Li, L. Cao, Z. Deng, R. Yu, High-pressure synthesis, crystal structure and physical properties of a new Cr-based arsenide La_3CrAs_5, Sci. China Mater. 63 (9) (2020) 1750–1758.

[16] J. Zhang, Y. Jia, X. Wang, Z. Li, L. Duan, W. Li, J. Zhao, L. Cao, G. Dai, Z. Deng, A new quasi-one-dimensional compound Ba_3TiTe_5 and superconductivity induced by pressure, NPG Asia Mater. 11 (2019) 60.

[17] J. Zhang, X. Wang, L. Zhou, G. Liu, D.T. Adroja, I. Dasilva, F. Demmel, D. Khalyavin, J. Sannigrahi, H.S. Nair, A ferrotoroidic candidate with well-separated spin chains, Adv. Mater. 34 (12) (2022) 2106728..

[18] L. Duan, X.C. Wang, J. Zhang, J.F. Zhao, W.M. Li, L.P. Cao, Z.W. Zhao, C. Xiao, Y. Ren, S. Wang, Doping effect on the structure and physical properties of quasi-one-dimensional compounds $Ba_9Co_3(Se_{1-x}S_x)_{15}$ (x = 0 – 0.2), Chin. Phys. B. 30 (2021) 106101.

[19] J. Zhang, A.C. Komarek, M. Jin, X. Wang, Y. Jia, J. Zhao, W. Li, Z. Hu, W. Peng, X. Wang, High-pressure synthesis, crystal structure, and properties of iron-based spin-chain compound $Ba_9Fe_3Se_{15}$, Phys. Rev. Mater.. 5 (2021) 054606.

[20] J. Zhang, M. Liu, X. Wang, K. Zhao, L. Duan, W. Li, J. Zhao, L. Cao, G. Dai, Z. Deng, $Ba_9V_3Se_{15}$: a novel compound with spin chains. *J. Phys.* Condens. Matter 30 (21) (2018) 214001.

[21] J. Zhang, X. Zhang, Y. Xia, J. Zhao, L. Duan, G. Wang, B. Min, H. Cao, C. R. Delacruz, K. Zhao, Structure and magnetic properties of $Ba_9V_3Te_{15}$ with ferromagnetic spin chains, Phys. Rev. B. 108 (2023) 174423.

[22] J. Zhang, R. Su, X. Wang, W. Li, J. Zhao, Z. Deng, S. Zhang, S. Feng, Q. Liu, H. Zhao, Synthesis, crystal structures, and electronic properties of one dimensional $Ba_9Sn_3(Te_{1-x}Se_x)_{15}$ (x = 0–1), Inorg. Chem. Front. 4 (8) (2017) 1337–1343.

[23] B. Almoussawi, H. Tomohiri, H. Kageyama, H. Kabbour, High pressure synthesis of the spin chain sulfide $Ba_9V_3S_{11}(S_2)_2$, Eur. J. Inorg. Chem. 2021 (2021) 1271.

[24] A. Abdeljalil, D. Shahab, S. Navid, K. Holger, Electronic structure and physical properties of the semiconducting polytelluride Ba_2SnTe_5 with a unique Te_5^{4-} unit, Chem. Mater. 16 (2004) 4193.

[25] S. Raman, P. G, M.I. Panneer, S.Y. Xu, M. Zahidhasan, F.C. Chou, , Crystal growth and transport properties of Weyl semimetal TaAs, *J. Phys.* Condens. Matter 30 (2018) 015803.

[26] S.M. Huang, S.Y. Xu, I. Belopolski, C.C. Lee, G. Chang, B. Wang, N. Alidoust, G. Bian, M. Neupane, C. Zhang, A. Weyl, Fermion semimetal with surface Fermi arcs in the transition metal monopnictide TaAs class, Nat. Commun. 6 (2015) 7373.

[27] B.Q. Lv, H.M. Weng, B.B. Fu, X.P. Wang, H. Miao, J. Ma, P. Richard, X.C. Huang, L. X. Zhao, G.F. Chen, Experimental discovery of Weyl semimetal TaAs, Phys. Rev. X. 5 (2015) 031013.

[28] C.G. Wang, Y. H, L.X. Zhao, G.F. Chen, K. Matano, R. Zhou, G.Q. Zheng, Landau diamagnetism and Weyl-fermion excitations in TaAs revealed by ^{75}As NMR and NQR, Phys. Rev. B. 101 (2020) 241110.